Acta Biochim Biophys Sin 2014, 46: 837–850 | © The Author 2014. Published by ABBS Editorial Office in association with Oxford University Press on behalf of the Institute of Biochemistry and Cell Biology, Shanghai Institutes for Biological Sciences, Chinese Academy of Sciences. DOI: 10.1093/abbs/gmu077.
Advance Access Publication 22 September 2014

Original Article

Structure variations of TBA G-quadruplex induced by 2′-*O*-methyl nucleotide in K^+ and Ca^{2+} environments

Xiaoyang Zhao[1,2], Bo Liu[1], Jing Yan[1], Ying Yuan[1], Liwen An[1], and Yifu Guan[1]*

[1]Key Laboratory of Medical Cell Biology, Ministry of Education, Department of Biochemistry and Molecular Biology, China Medical University, Shenyang 110001, China
[2]Department of Chemistry, Shenyang Medical College, Shenyang 110034, China
*Correspondence address. Tel/Fax: +86-24-23255240; E-mail: yfguan55@sina.com

Thrombin binding aptamer (TBA), a 15-mer oligonucleotide of d(GGTTGGTGTGGTTGG) sequence, folds into a chair-type antiparallel G-quadruplex in the K^+ environment, and each of two G-tetrads is characterized by a *syn–anti–syn–anti* glycosidic conformation arrangement. To explore its folding topology and structural stability, 2′-*O*-methyl nucleotide (OMe) with the *C3′-endo* sugar pucker conformation and *anti* glycosidic angle was used to selectively substitute for the guanine residues of G-tetrads of TBA, and these substituted TBAs were characterized using a circular dichroism spectrum, thermally differential spectrum, ultraviolet stability analysis, electrophoresis mobility shift assay, and thermodynamic analysis in K^+ and Ca^{2+} environments. Results showed that single substitutions for *syn*-dG residues destabilized the G-quadruplex structure, while single substitutions for *anti*-dG residues could preserve the G-quadruplex in the K^+ environment. When one or two G-tetrads were modified with OMe, TBA became unstructured. In contrast, in Ca^{2+} environment, the native TBA appeared to be unstructured. When two G-tetrads were substituted with OMe, TBA seemed to become a more stable parallel G-4 structure. Further thermodynamic data suggested that OMe-substitutions were an enthalpy-driven event. The results in this study enrich our understanding about the effects of nucleotide derivatives on the G-quadruplex structure stability in different ionic environments, which will help to design G-quadruplex for biological and medical applications.

Keywords TBA; structure variation; nucleotide derivative; ionic environment

Received: February 12, 2014 Accepted: July 16, 2014

Introduction

Guanine-rich sequences are able to fold into an unusual secondary structure called G-quadruplex (G-4). The G-4 structure contains two or more stacked G-tetrads, and each G-tetrad is composed of four guanine residues maintained together by Hoogsteen hydrogen bonds in a plane. Based on the relative strand directions, these G-4s can be classified into parallel or antiparallel topology (**Fig. 1**). These highly ordered G-4 structures have been frequently found in telomeres [1–3], gene promoters [4,5], and the 5′-untranslated regions of mRNAs [6,7] of eukaryotic systems, implying their biological functions in oncogenetics and transcription/translation regulations [8,9].

Synthetic guanine-rich oligonucleotides are able to fold into particular G-4 structures. One of the extensively studied examples is thrombin binding aptamer (TBA). TBA is a 15-mer oligonucleotide of d(GGTTGGTGTGGTTGG). It interacts with thrombin in a high binding affinity to inhibit the thrombin-catalyzed process of fibrinogen–fibrin conversion. Structural analyses show that TBA folds into a chair-type antiparallel G-4 structure in K^+ solution [10,11] (**Fig. 1**). One of the particularly interesting features of this G-4 structure is that the guanine residues in the G-tetrads adopt different glycosidic angles: G2, G6, G11, and G15 are in the *anti* glycosidic angle, while G1, G5, G10, and G14 are in the *syn* glycosidic angle. Thus, each G-tetrad is characterized by a *syn–anti–syn–anti* glycosidic angle arrangement [12,13].

Many studies have been carried out to understand the folding topology and structural stability of TBA. One of the strategies is to use different nucleotide derivatives with specific structural features or physicochemical properties to selectively substitute nucleotides of TBA. As shown in **Fig. 2**, deoxyribonucleotides (DNA residues) have a *C2′-endo* sugar pucker conformation, whereas ribonucleotides (RNA residues) have a *C3′-endo* sugar pucker conformation. Many nucleotide derivatives of a particular structure offer many opportunities and advantages for this purpose. For example, locked nucleic acid (LNA) has a well-confined *C3′-endo* sugar pucker conformation and an *anti* glycosidic bond angle due to its bicyclic ring furanosyl structure [14]. In

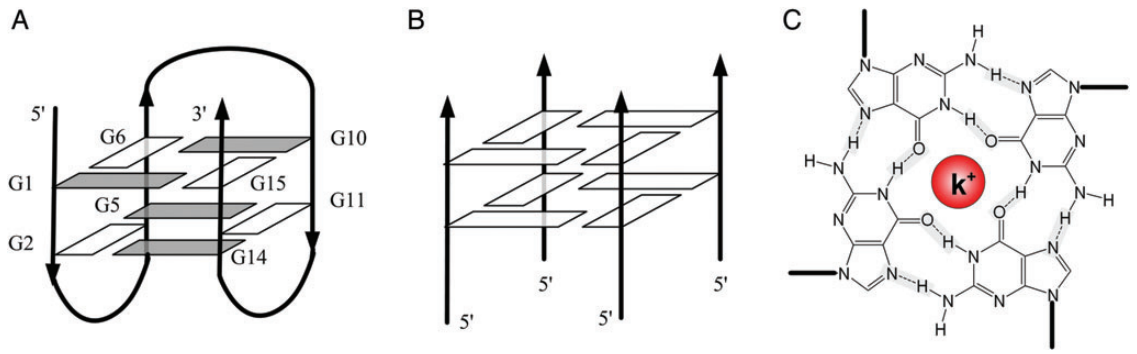

Figure 1. Spatial structure of G-quadruplex (A) Antiparallel G-quadruplex of TBA. (B) Parallel G-quadruplex. (C) A G-tetrad plan with a coordinated K^+ in the center. Gray and white colors represent *syn* and *anti* glycosidic conformations, respectively.

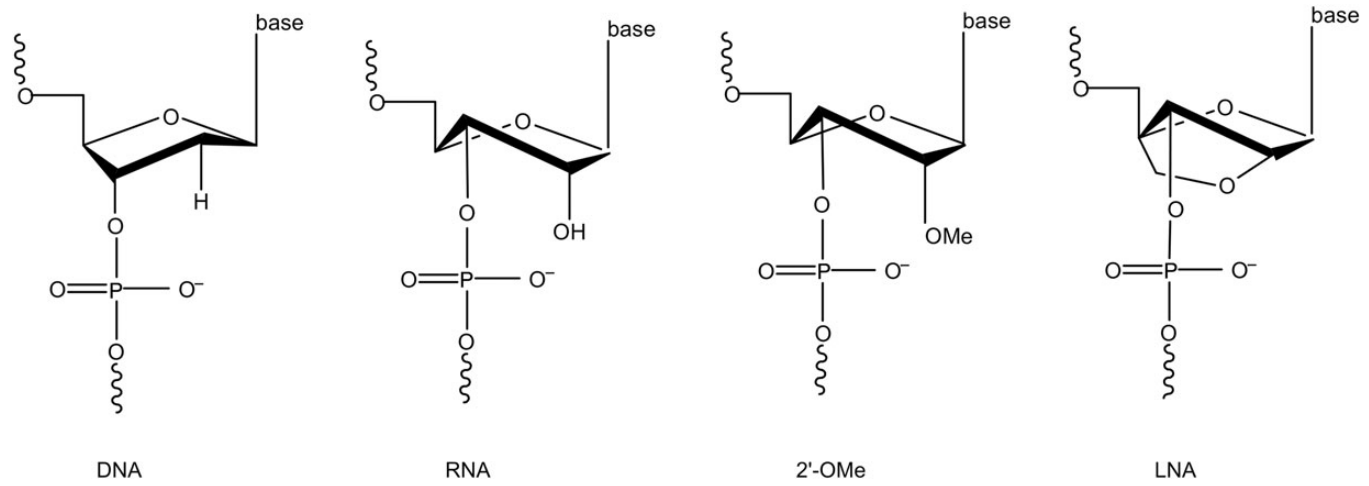

Figure 2. Chemical structures of DNA, RNA, 2′-OMe, and LNA DNA is in the C2′-*endo* sugar pucker conformation, while others are in the C3′-*endo* sugar pucker conformation.

comparison, unlocked nucleic acid (UNA) exhibits a less rigid sugar pucker conformation because of the missing bond between C2′ and C3′ atoms [15,16]. Furthermore, 2′-deoxy-2′-fluoro-β-D-arabinonucleic acid (2′F-ANA) [17] and 8-bromodexoyguanine (8-BrdG) [18,19] possess different sugar pucker rigidity and glycosidic angles. The modified TBAs using these different nucleotide derivatives have been studied using nuclear magnetic resonance (NMR) spectroscopic analyses, circular dichroism (CD) measurements, ultraviolet (UV) thermal stability determination as well as anticoagulant assay, and the effects of sugar pucker conformation, glycosidic angles, the loop−ion interactions on the TBA G-4 structures have also been explored.

2′-*O*-Methyl nucleotide (OMe) is another nucleotide derivative with a modified ribose, which possesses a *C3′-endo* sugar pucker conformation and a constrained *anti* glycosidic bond angle (**Fig. 2**) [20]. It exhibits many attractive properties, such as preference to hybridize with RNA sequences, faster hybridization kinetics than DNA [21,22], excellent biological stability, and biocompatibility useful for antisense-based therapeutic applications [23−25]. Thus, it could be used as an alternative model compound to study how a particular structural conformation of individual nucleotides affects the TBA G-4 structure stability and relevant biological functions. Compared with other derivatives, OMe-substituted TBA has not been explored yet. In addition, TBA has been studied in K^+ and Na^+ solutions in previous studies [26,27], but systematic substitutions of TBA with OMe in K^+ and Ca^{2+} environments have not been reported, and the effect of divalent ions on the TBA G-4 folding topology remains unclear.

In this study, we prepared a group of TBA variants which contain one, two, four, or eight OMe-substitutions at the selected positions, and characterized their G-4 topologies in both K^+ and Ca^{2+} environments by CD spectroscopy, thermal differential spectrum (TDS), UV thermal stability analysis, and non-denatured electrophoresis mobility shift assay. We then proposed a possible TBA folding topology for each TBA variant and discussed its unique formation in different ionic environments.

Materials and Methods

Preparation of oligonucleotides

The native TBA and OMe-substituted TBAs (HPLC grade) were purchased from TaKaRa (TaKaRa, Dalian, China). Their stock solutions were prepared in 10 mM sodium cacodylate buffer (pH 7.5) at a final concentration of 0.1 mM and stored at −20°C.

TBAs containing one, two, four, and eight OMe-substitutions at the selected positions were prepared by Sangon Biotech (Shanghai, China) (**Table 1**). Their solutions were prepared in 10 mM sodium cacodylate buffer (pH 7.5), containing either 50 mM KCl or 50 mM $CaCl_2$.

CD spectroscopy

CD spectra of TBA species were acquired using a Jasco J-810 spectropolarimeter (Jasco, Tokyo, Japan). A total of 500 μl of TBA solution in a cell of 0.1 cm path length was placed in a thermo stable holder. CD spectra were recorded from 200 to 340 nm at room temperature unless specified. Three scans at a speed of 500 nm/min were accumulated for each sample. The final TBA concentration (5 μM) for CD spectroscopic study was prepared in 10 mM sodium cacodylate buffer (pH 7.5), containing either 50 mM KCl or $CaCl_2$. To ensure that all TBAs adopt the same structure at the beginning of each experiment (CD measurement, UV analysis, TDS and native gel electrophoresis), a slow melting-cooling cycle at 0.2°C/min was performed prior to each experiment. The native TBA and OMe-modified TBAs with identical sequences were assumed to have identical extinction coefficients.

To examine the structural stability, CD spectra of the native TBA dissolved in 50 mM KCl buffer were recorded at different temperatures. The temperature of the sample was controlled using a circulating water bath (Pharmacia, Stockholm, Sweden). Samples were equilibrated at each temperature for 5 min prior to data acquisition. The ellipticity was calculated using the software Spectra Manager.

Table 1. Nucleotide sequences of TBA and OMeN-modified TBAs

Name	Modified TBA sequence
TBA	5′d(GGTTGGTGTGGTTGG)
M1(2)	5′d(G**g**TTGGTGTGGTTGG)
M1(5)	5′d(GGTT**g**GTGTGGTTGG)
M1(11)	5′d(GGTTGGTGTG**g**TTGG)
M1(14)	5′d(GGTTGGTGTGGTT**g**G)
M2(2,11)	5′d(G**g**TTGGTGTG**g**TTGG)
M2(5,11)	5′d(GGTT**g**GTGTG**g**TTGG)
M2(10,11)	5′d(GGTTGGTGT**gg**TTGG)
M2(11,14)	5′d(GGTTGGTGTG**g**TT**g**G)
M4(2,5,11,14)	5′d(G**g**TT**g**GTGTG**g**TT**g**G)
M8(1,2,5,6,10,11,14,15)	5′d(**gg**TT**gg**TGT**gg**TT**gg**)

*DNA and OMeN are in upper and lower cases, respectively. Numbers in parentheses are the modified positions of TBA nucleotide sequence. TBA M1(*n*)s represent a single OMe substitution at the position *n* (*n* = 2, 5, 11, or 14) of TBA, respectively. Similarly, TBA M2 represents the TBA species containing two OMe substitutions. M2(2,11) indicates two OMe substitutions at diagonal positions 2 and 11 in the same G-tetrad plane, M2(5,11) and M2(11,14) have two OMe substitutions at adjacent positions in the same G-tetrad plane, and M2(10,11) has two OMe-substitutions at the stacked positions in two tetrad planes. TBA M4 and M8 represent four OMe substitutions in one G-tetrad plane and eight substitutions in two G-tetrad planes, respectively.

Thermal stability analysis

The UV absorption melting curves of different TBA species were recorded on a UV−VIS spectrophotometer equipped with a Cary 100 temperature control accessory (Varian, Salt Lake City, USA). Eighty microliters of TBA solution in a capped quartz cuvette of 1.0 cm path length were used in each measurement. To make the experimental data comparable, a multicell thermal block was used to make temperature measurement for six samples simultaneously. The UV absorption at 295 nm was measured at temperatures ranging from 25 to 90°C with 1.0°C increment. It has been well known that the absorbance at 295 nm allows precise monitoring of the G-quadruplex unfolding and folding processes [28]. To ensure that the structural transition of TBA was conducted under a thermal equilibrium condition, a slow rate of 0.2°C/min was used for both heating and cooling processes. The denaturation and renaturation curves for data analysis were an average of three independent measurements. The hysteretic behavior of the melting/annealing process was used to evaluate the kinetics of G-4 formation. To assess the molecularity of the G-4 formation, the dependence of the thermal stabilities on the oligonucleotide concentration was examined. The structurally stable TBA variants at concentrations of 0.1, 0.5, 1.0, 5.0, and 10.0 μM in K^+ and Ca^{2+} solutions were recorded using the same data acquisition procedure mentioned above.

Thermal differential spectrum (TDS)

Absorption spectra of each substituted TBA species were recorded on a Cary 100 UV−VIS spectrophotometer (Varian) in the range from 200 to 340 nm with a scan speed of 1200 nm/min and a spectral increment of 1 pt/nm. These spectra were collected at temperatures of 90 and 15°C, which corresponds to the unfolded and folded states, respectively. Thermal differential spectra were obtained by subtraction of the low temperature (15°C) absorbance spectra from the high temperature (90°C) absorbance spectra. All of the differential spectra were normalized.

Thermodynamic parameters calculation

The absorbance profile recorded at 295 nm was analyzed using the built-in software Cary WinUV which is designed based on the principle of non-linear least-square curve fitting and van't Hoff plot method [29].

The best-fit baselines of melting curves before and after thermal transition were obtained using the non-linear least-square curve fitting approach and then normalized using the following formula:

$$\theta T = (A(T) - A_{\mathrm{U}}(T))/(A_{\mathrm{F}}(T) - A_{\mathrm{U}}(T),$$

where θ is the folded fraction of G-4 at a given temperature, $A(T)$, $A_{\mathrm{U}}(T)$ and $A_{\mathrm{F}}(T)$ represent the UV absorbance at a given temperature, the unfolded UV absorption and the folded UV absorption at 295 nm, respectively. The folded fraction curves lead to the determination of the melting temperature (T_{m}) and the annealing temperature (T_{a}), which correspond to the point of $\theta = 0.5$ [30]. These normalized melting curves were used to assist the calculation of the thermodynamic parameters (ΔH, ΔS, and ΔG) once the concentration of oligonucleotide, molecularity, and the calculation temperature were given [30]. In general, the analysis assumes that ΔH is independent of temperature, which means that the heat capacity change (ΔCp) during the reaction is zero. Standard ΔH and ΔS were used to determine the Gibbs energy and the association constant (K_{a}). K_{a} was obtained using the formula $K_{\mathrm{a}} = \theta/(1-\theta)$, and $\ln(K_{\mathrm{a}})$ was plotted as a function of $1/T$ in K^{-1}. By using the equation of free Gibbs energy $\Delta G = -RT\ln(K_{\mathrm{a}}) = \Delta H - (T\Delta S)$, $\ln(K_{\mathrm{a}})$ could be equal to $-(\Delta H/R)\cdot(1/T)+\Delta S/R$. The plot of $\ln(K_{\mathrm{a}})$ versus $1/T$ is a straight line with a slope of $-\Delta H/R$ and an intercept on Y axis of $\Delta S/R$. In the current study, all the original experimental curves for data processing were an average of at least three independent measurements and the accuracy of T_{m} and T_{a} values was within ± 0.1°C.

Electrophoresis mobility shift assay

OMe-substituted TBA species were incubated with 10 mM sodium cacodylate buffer (pH 7.5) in the presence of 50 mM KCl or $CaCl_2$ at 37°C for 1 h. Then, 20% native gels were prepared by mixing 13.3 ml 30% acrylamide solution, 4 ml 5 × TB (containing 50 mM KCl or $CaCl_2$), 2.5 ml water, 140 μl 10% APS, and 13 μl TEMED. The gel of 8 cm × 10 cm × 0.1 cm was polymerized within 45 min. A final concentration of 20 μM TBA solutions (containing 2 μl stock solution, 2 μl loading buffer, 1 μl 1 M KCl or $CaCl_2$, and 5 μl water) was loaded on gels. Electrophoresis was run in 1 × TB (Tris-borate buffer containing 50 mM KCl or 50 mM $CaCl_2$) for 1.5 h at 100 V at 4°C. The gels were then stained with Stains-All (Sigma) and washed three times. Images were recorded using a Model Z320 Personal Scanner (FangZheng, Beijing, China).

Results

G-4 folding topology of OMe-substituted TBA in K^+ solution

To confirm the folding topology of the native TBA, its CD spectrum was recorded using the procedure as described previously [31]. As expected, in 50 mM K^+ solution, it showed a characteristic CD spectrum of an antiparallel G-4 structure: positive peaks at 295 and 245 nm as well as a negative peak at 265 nm (**Fig. 3A**) [32]. As the temperature increased, these CD peaks were gradually decreased, and finally its CD spectrum became featureless, indicating that the antiparallel G-4 structure of native TBA has been changed to an unstructured oligonucleotide at a high temperature (**Fig. 3B**). These CD spectra were consistent with the previous results [31] and served as an important reference for comparison with CD spectra of other OMe-substituted TBAs.

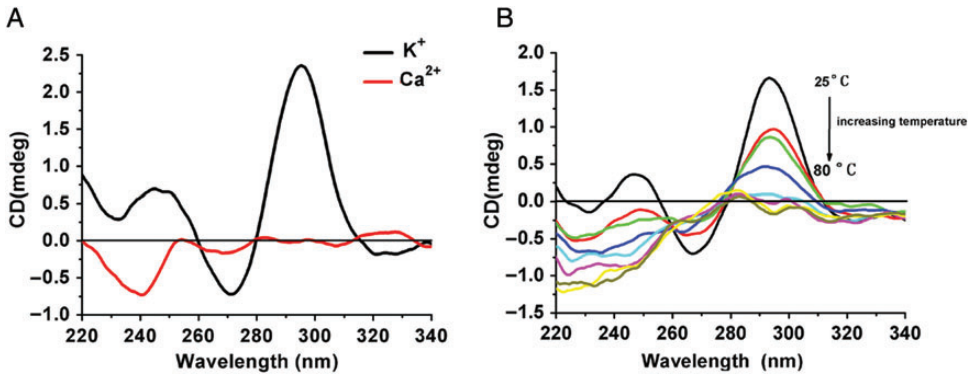

Figure 3. CD spectra of the native TBA in K^+ and Ca^{2+} solutions and in the K^+ solution at different temperatures (A) CD spectra of TBA in K^+ and Ca^{2+} solutions, respectively. Each CD spectrum is an average of at least three scans. A CD maximum at 295 nm and a CD minimum at 265 nm are spectral signatures of the anti-parallel G-quadruplex structure of TBA. The TBA concentration is 5 μM in 10 mM sodium cacodylate (pH 7.5). (B) CD spectra of the native TBA in the K^+ solution at different temperatures. As the temperature increases, the CD maximum at 295 nm and the CD minimum at 265 nm become disappeared gradually, indicating the collapse of the anti-parallel G-quadruplex of the native TBA.

OMe-substituted TBA species M1(2) and M1(11) showed the CD spectra almost identical to the native TBA (**Fig. 4A**), suggesting that they have the same G-4 folding topology as the native TBA. However, the CD peaks of M1(5) and M1(14) were significantly reduced, indicating much unstable G-4 structures. The CD spectra of M2(2,11), M2(5,11), M2(10,11), and M2(11,14) were almost featureless, implying an unstructured oligonucleotide (**Fig. 4B**). The CD spectra of species M4(2,5,11,14) and M8(1,2,5,6,10,11,14,15) clearly suggested that they are unstructured (**Fig. 4C**).

The thermal differential spectrum of native TBA exhibited two negative peaks at 265 and 295 nm, and two positive peaks at 245 and 275 nm (**Fig. 5A**), which were the typical TDS signatures of antiparallel G-4 structure previously reported [33]. Only M1(2) and M1(11) displayed a similar TDS feature (**Fig. 5A**). Other OMe-substituted M2, M4, and M8 did not show any TDS features except M2(2,11) (**Fig. 5B,C**), implying unstructured oligonucleotides.

G-4 folding topology of OMe-substituted TBA in Ca^{2+} solution

The CD spectrum of the native TBA in 50 mM Ca^{2+} solution was an almost flat curve, except a negative peak at around 240 nm (**Fig. 3A**). In addition, the native TBA showed a

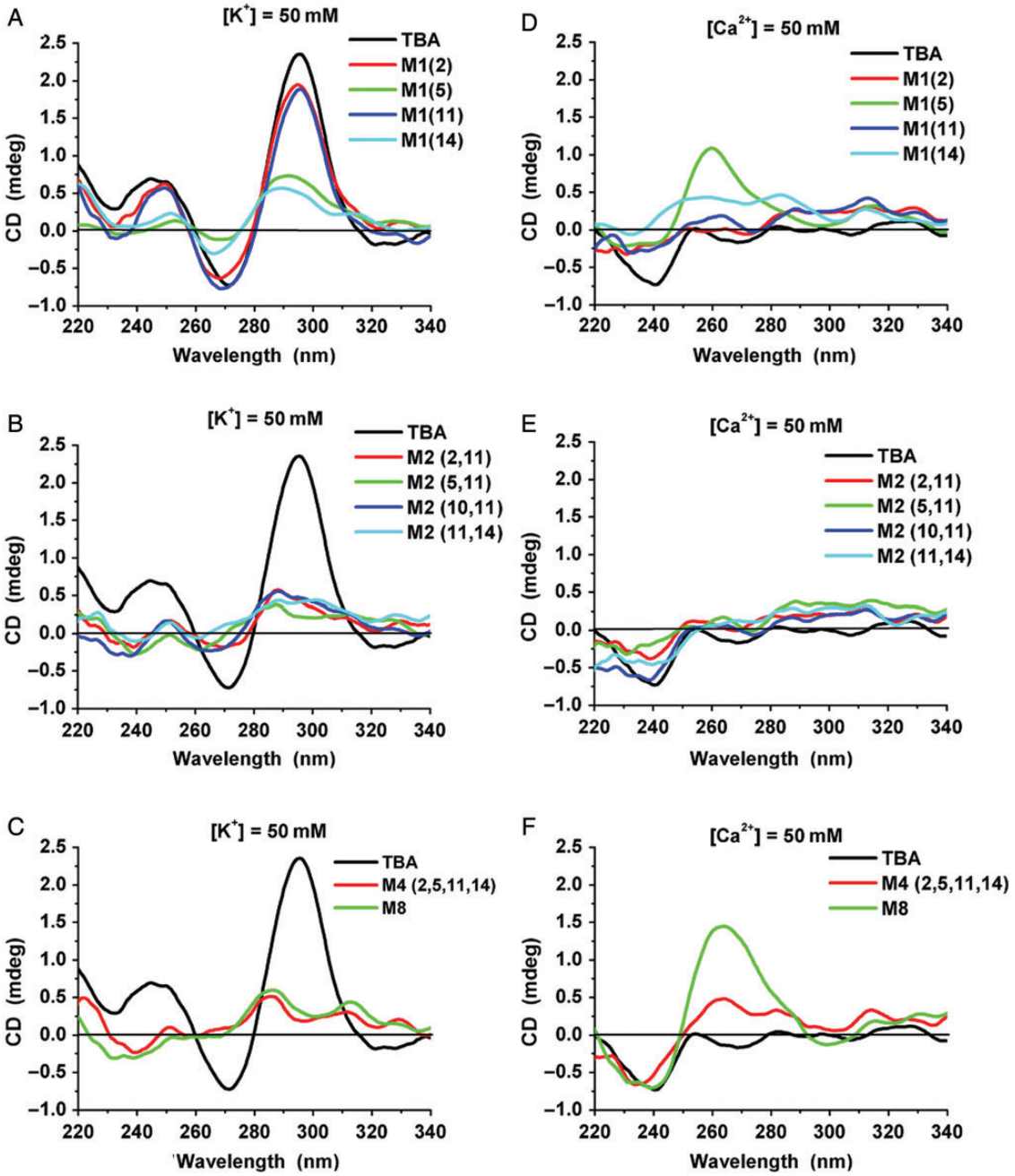

Figure 4. CD spectra of native and 2′-OMe-substituted TBAs in 50 mM K^+ (left) and 50 mM Ca^{2+} environments (right) (A,D) Single substitution. (B,E) Double substitution. (C,F) Four and eight substitution.

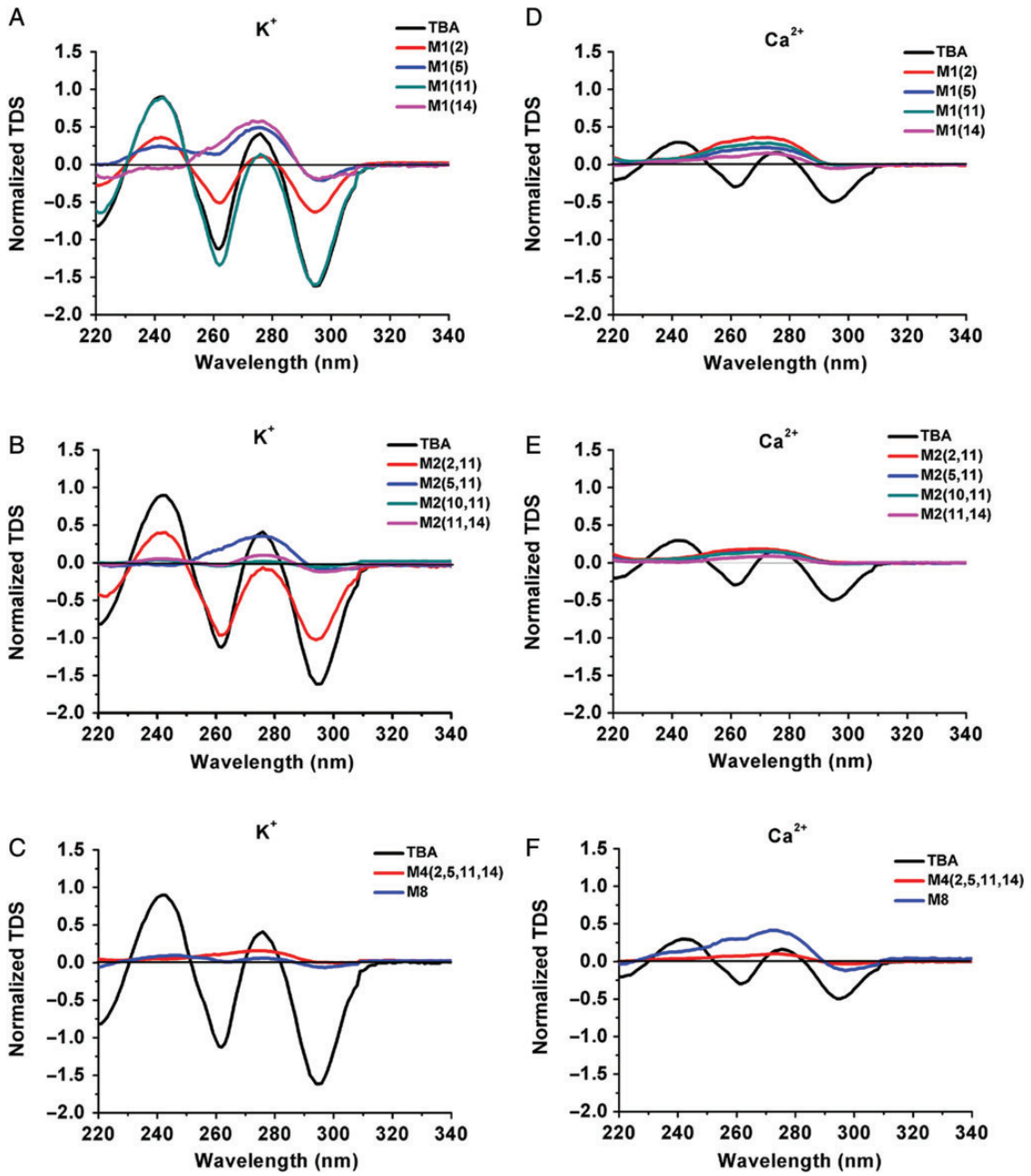

Figure 5. Normalized TDS of native and 2′-OMe-substituted TBAs in 50 mM K^+ (left) and 50 mM Ca^{2+} environments (A,D) Single substitution. (B,E) Double substitution. (C,F) Four and eight substitution.

weak TDS feature (**Fig. 5D**). These data suggested that the native TBA in 50 mM Ca^{2+} solution might have some local structures due to the loop−ion interaction. Single-OMe-substituted species, M1(2), M1(11), and M1(14), also showed featureless CD spectra (**Fig. 4D**). Interestingly, the CD spectrum of M1(5) showed a positive peak at ~265 nm (**Fig. 4D**). Double substitutions did not promote TBA to become structured (**Fig. 4E**). However, when two G-tetrads were fully substituted, M8 showed a CD spectrum characteristic of a stable parallel G-4 structure (**Fig. 4F**).

Electrophoresis mobility shift of OMe-substituted TBAs

To prove the structural variations induced by OMe-substitutions in different ionic environments, we analyzed these OMe-substituted TBAs by non-denatured polyacrylamide gel electrophoresis mobility shift assay. The running buffers contained 50 mM K^+ or 50 mM Ca^{2+}, respectively, to maintain the original structures of these substituted TBAs. To minimize the temperature effect, electrophoresis experiments were performed at 4°C. Using 8-bp and 16-bp oligonucleotides as the mobility markers, we found that the native TBA migrated at a

rate comparable to a 10-bp oligonucleotide in K^+-containing gel. The OMe-substituted TBAs ran differently due probably to their structure variations. The unstructured M8 migrated at a rate similar to a 14-bp oligonucleotide, slower than others because of its extended chain (**Fig. 6A**). It is worth noting that all these native TBA and OMe-substituted TBAs showed a single band, implying that only one type of TBA conformer was present in each case.

In Ca^{2+}-containing gel, the native TBA moved at a rate of a 14-bp oligonucleotide just like M8 in the K^+-containing gel. The substituted M8 was significantly retarded, slower than the 16-bp oligonucleotide (**Fig. 6B**). Other partially substituted TBAs ran at the rates between the native TBA and M8. In all, each TBA in the Ca^{2+}-containing gel showed only one band except M1(5) and M4(2,5,11,14) which showed one dominant band and one very weak band.

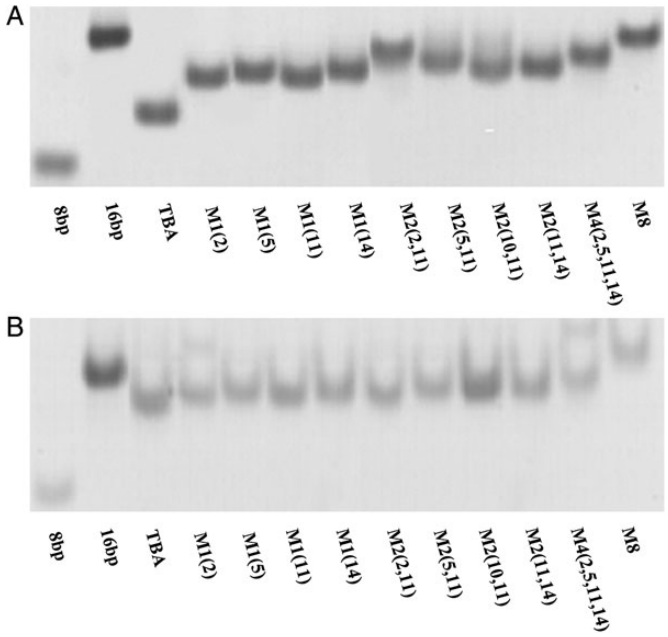

Figure 6. Native PAGE images of the TBA and OMe-substituted TBAs in 50 mM electrophoresis buffer (A) KCl. (B) $CaCl_2$.

UV thermal analysis of structural stability of OMe-substituted TBAs

The melting curves at 295 nm were recorded for all TBA species, and melting temperatures (T_m) were determined accordingly. A slower heating/cooling rate (0.2°C/min) was applied to ensure that these thermal transition processes were under thermal equilibrium conditions. There are two ways to determine the melting temperature: normalization of the melting curve and the first derivative of the melting curve. In this study, we used the folded fraction correction to normalize these curves for data analysis [34]. The melting temperatures determined using the first derivative of melting curve were less consistent and were not used in this study. In addition, we also recorded their annealing curves and determined their annealing temperatures (T_a).

The melting curve and annealing curve of the native TBA in K^+ solution were perfectly reversible (**Supplementary Fig. S1**), and T_m was determined to be 50.2°C (**Table 2**). In the case of single OMe substitution for *anti*-dG, the melting and annealing curves of M1(2) were almost reversible with T_m and T_a of 38.7 and 38.1°C, respectively. M1(11) also showed a similar reversible feature with T_m and T_a of 38.8 and 38.2°C, respectively (**Fig. 7**). These results are consistent with the CD data (**Fig. 4A**). Once the *syn*-dG residues were substituted, M1(5) and M1(14) demonstrated very small UV absorbance changes without obvious thermal transition, indicating that they were much less stable. These data are consistent with that of CD analysis (**Fig. 4B**) and TDS results (**Fig. 5B**). M2(5,11), M2(2,11), M2(10,11), and M2(11,14) showed flat UV absorption curves, indicating an unstructured oligonucleotide. The UV spectrum of M4 and M8 became almost flat, and no thermal transition could be determined (**Supplementary Fig. S1**).

In contrast, the native TBA showed no thermal transition at all in Ca^{2+} environment (**Supplementary Fig. S2**). M1(5) showed a minor thermal transition, and its melting and annealing curve were not reversible. All M2 species did not show any obvious thermal transition. However, M4 exhibited an evident non-reversible behavior of the melting and annealing curves, and its T_m and T_a were estimated to be

Table 2. Melting temperature, annealing temperature, and thermal parameters (25°C of TBA and OMeN-substituted TBAs in K^+ and Ca^{2+} solutions

Ions	Species	T_m (°C)	ΔH (kJ/mol)	TΔS (kJ/mol)	ΔG (25 °C) (kJ/mol)	T_a (°C)
K^+	TBA	50.2 ± 0.1	−216.6 ± 1.0	−199.6 ± 0.7	−16.95 ± 0.1	49.5 ± 0.1
	M1(2)	38.7 ± 0.1	−151.2 ± 1.2	−144.6 ± 1.4	−6.652 ± 0.1	38.1 ± 0.0
	M1(11)	38.8 ± 0.0	−151.5 ± 0.9	−144.8 ± 1.1	−6.696 ± 0.4	38.2 ± 0.0
	M2(2,11)	29.3 ± 0.1	−139.0 ± 2.1	−136.9 ± 1.9	−1.955 ± 1.9	28.9 ± 0.0
Ca^{2+}	M4	53.2 ± 0.0	−215.6 ± 1.2	−196.9 ± 2.9	−18.651 ± 0.1	33.1 ± 0.0
	M8	60.3 ± 0.1	–	–	–	45.6 ± 0.0

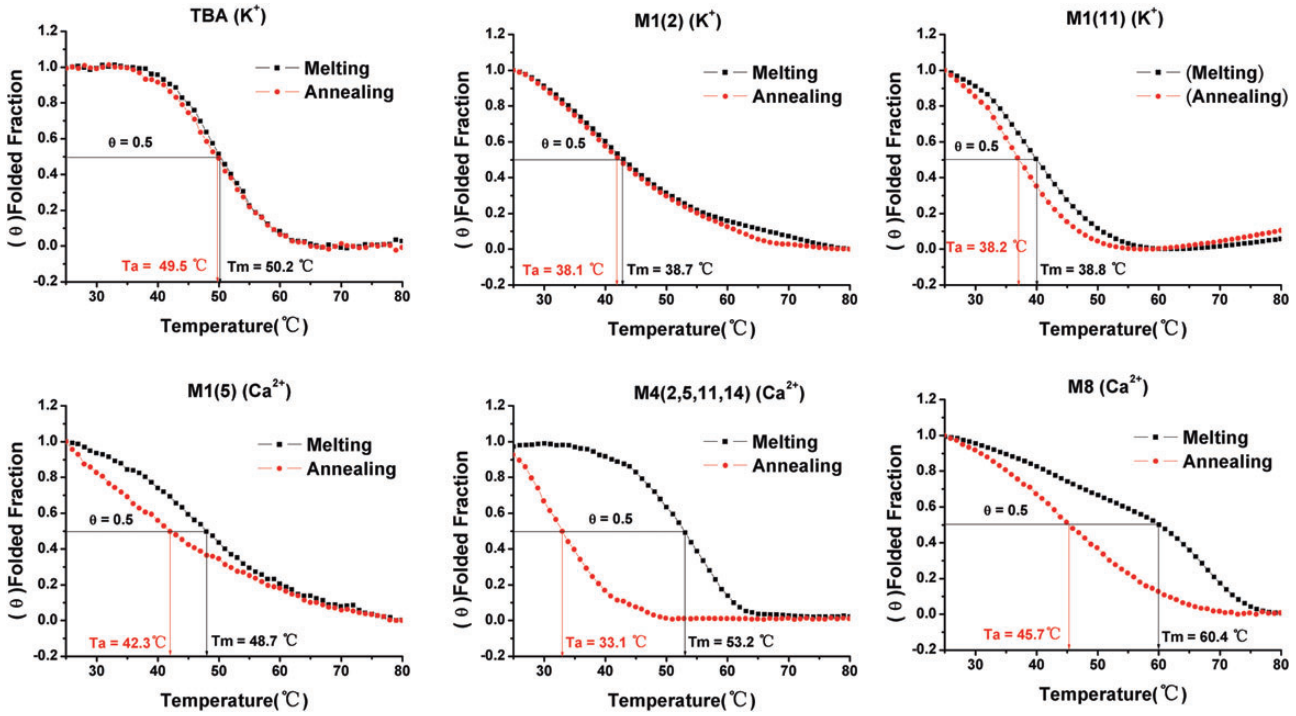

Figure 7. Calculated folded fraction curves T_m and T_a represent melting temperature and annealing temperature, respectively.

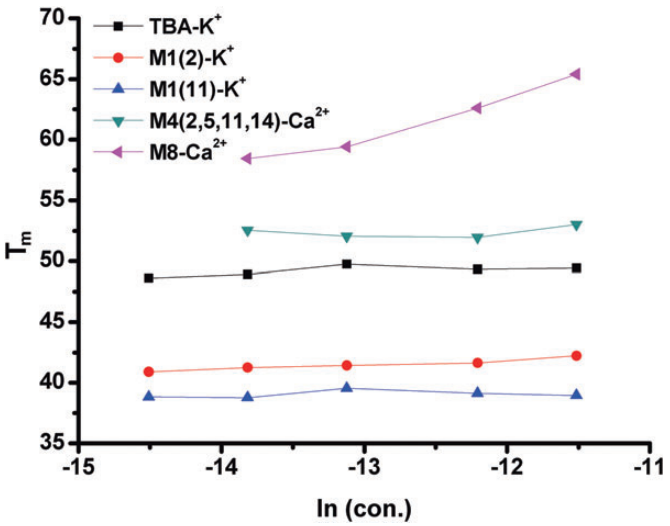

Figure 8. Concentration-dependent behavior of melting temperatures of TBA and OMe-substituted TBAs

53.2 and 33.1°C, respectively (**Fig. 7**). The hysteretic behavior implied that, in Ca^{2+} environment, M4 underwent different denaturation and renaturation processes, but could also be the result of the mixture of two different species. M8 presented a complex melting curve of a multiple-phase thermal transition.

To determine the molecularity of these OMe-modified TBAs, the melting temperatures of TBA, M1(2) and M1(11) in K^+ solution and M4 and M8 in Ca^{2+} solution at concentrations of 0.1, 0.5, 1.0, 5.0, and 10.0 μM were also recorded. The concentration >10.0 μM was not used in this study because higher concentrations might raise concern about the correctness of very intense UV absorption. Melting temperatures of M4 and M8 at a concentration of 0.1 μM in Ca^{2+} solution were not determined since their UV melting curves were too noisy. These plots showed that only M8 demonstrated a concentration-dependent melting temperature profile in Ca^{2+} solution (**Fig. 8**).

Discussion

To determine the definitive folding topologies of G-quadruplexes of different G-rich sequences under different conditions, X-ray crystallographic and NMR spectroscopic methods have been utilized extensively, and many G-quadruplex structural features (strand polarity, molecularity, loop orientations, and so on) have been observed [10,13,35]. To explore the effects of hydrogen bonds, G-tetrad stacking interactions, glycosidic angles, and ion binding sites on the G-quadruplex formation, many nucleotide derivatives have been used to substitute for special nucleotides of these G-quadruplexes. CD spectroscopy, as a supplementary approach to X-ray crystallographic and NMR spectroscopic methods, offers advantages of easy sample preparation, data acquisition, and structure interpretation to identify the G-quadruplex structures [36,37]. Previous studies have derived empirical CD spectral signatures characterizing particular G-4 topologies. In general, an antiparallel G-4

topology exhibits two positive peaks (~295 and 245 nm) and a negative peak at ~265 nm [32,38]. On the other hand, the parallel G-4 structure displays usually a positive peak at ~265 nm and a negative peak at ~240 nm [38,39]. When the G-rich sequences adopt a hybrid G-4 structure, their CD spectra show a mixed profile of antiparallel and parallel G-4 structure [38,40]. These CD spectroscopic signatures have been used as a convenient means to distinguish different G-4 topologies, particularly when the structural information of X-ray crystallography and NMR spectroscopy are not available.

Prediction of the G-4 folding topologies presents a great challenge, since accumulated data have shown that the G-rich sequences, molecularity, loop property, and ionic condition can significantly influence the G-4 folding topology and structural stability. In addition, the sugar pucker conformations and the glycosidic angles of nucleotides in the G-tetrads also play an important role.

To uncover the relationship of the TBA G-4 structure with the sugar pucker conformations and the specific glycosidic angle, many nucleotide derivatives with particular structural features have been studied. UNA is an acyclic RNA mimic with a missing bond between the *C*2′ and *C*3′ atoms of the ribose, thus, it can offer an increased sugar conformation flexibility. All 15 TBA variants with a single UNA substitution at each position showed similar CD spectra in 100 mM K^+ solution, indicating that UNA substitutions did not alter the original antiparallel G-4 topology at all [41]. It seemed that UNA substitutions for any nucleotides of TBA would not disturb the original glycosidic angle arrangement of G-tetrad.

In contrast, nucleotides having a well-confined sugar pucker conformation demonstrated significantly different effects on the G-4 folding topology. 2′-Deoxy-2′-fluoro-D-arabinonucleic acids (2′F-ANA) confer a DNA-like conformation and favor an *anti* glycosidic angle [42]. When the *anti*-dG residues of TBA were substituted with 2′F-araG, the antiparallel G-4 topology was still conserved. However, when all the *syn*-dG residues, two G-tetrads, and all residues were substituted with 2′F-ANA, their CD spectra presented a typical parallel G-4 topology in 25 mM K^+ solution. LNA is characterized by a 2′-*O*, 4′-C-methylene-β-D-ribofuranosyl unit. It is a bicyclic ribosyl structure that effectively 'locks' the ribose in the *C3′-endo* sugar pucker conformation that is dominant in A-form DNA and RNA [43]. This *C3′-endo* sugar conformation has a confined *anti* glycosidic angle. Bonifacio *et al*. [14] have measured the biological activity of LNA-modified TBA in 50 mM K^+ buffer, and found that single LNA substitution for either dG5, dT7, or dG8 showed the decreased thrombin inhibitory activity, whereas a LNA substitution for dG2 exhibited a biological activity comparable with the native TBA. In light of the glycosidic angle arrangement, the LNA-dG2 substitution maintained the original *syn*–*anti*–*syn*–*anti* glycosidic angle arrangement of the TBA G-tetrad, whereas the LNA-dG5 substitution induced the *syn*–*anti* switch of glycosidic angle. Virno *et al*. [36] used an NMR technique to analyze four LNA-substituted TBAs: single substitution for dG15 (LNA-dG15), single substitution for dG1 (LNA-dG1), eight substitutions of two G-tetrads and 15 substitutions of whole TBA nucleotides. The NMR results showed that LNA-dG15 turns out to be the only one that is able to form an antiparallel G-4 structure in K^+ buffer, while LNA-dG1 and TBA with eight LNA substitutions gives the spectra characteristic of a mixture of different G-4 structures. The fully substituted TBA was unstructured. It is apparent that only LNA-dG15 substitution would maintain the original *syn*–*anti*–*syn*–*anti* glycosidic angle arrangement, whereas others would not. A CD denaturation experiment also showed that the LNA-substituted sequence d(ggTTggTGTggTTgg) reduced the thermal stability by 20°C in comparison with the native TBA [36,44]. In constrast, when nucleotide derivatives possess a constrained *syn* glycosidic angle, their substitutions display an opposite effect. Good examples include 8-bromodeoxyguanine (8-BrdG) [19] and deoxyguanosine with bicycle(3.1.0)hexane pseudosugar [37].

Substitutions of ribonucleotides for deoxyribonucleotides of TBA has been studied by Tang and Shafer [45]. In 25 mM K^+ solution, dTBAr2 (GgTTGgTGTGgTTGg) preserved the same antiparallel G-4 topology, whereas dTBAr1 (gGTTgGTGTgGTTgG) became a parallel G-4 structure. The fully substituted species rTBA (gguuggugugguugg) demonstrated a CD spectrum of a parallel G-4 structure. These results concluded that the preference of riboguanosine for the *anti* glycosidic angle is the driving force for topology transition. Additionally, the thermal melting temperature versus the species concentration suggested that when the antiparallel G-4 structure of TBA was converted to a parallel one, the G-4 molecularity changed from a unimolecular one to a bimolecular one.

In the current study, we used OMe to further extend the understanding on the TBA G-4 folding topology influenced by the sugar pucker conformation and the glycosidic angle. As mentioned earlier, OMe is one of the RNA mimics with *C3′-endo* sugar pucker conformation and a constrained *anti* glycosidic angle. CD spectrum and TDS of each TBA species provided clear evidence of the TBA folding topology. When the *anti*-dG residues are substituted with OMe, M1(2) and M1(11) preserve the original *anti*–*syn*–*anti*–*syn* glycosidic conformation arrangement, and as expected, their CD spectra reveal an antiparallel G-4 topology of TBA. In the case of M1(5) and M1(14), however, their CD spectral peaks decrease significantly. In either of these two cases, OMe substitution leads to a *syn*–*anti* glycosidic angle switch of the substituted dG residues, and the resulting *syn*–*anti*–*anti*–*anti* or *anti*–*anti*–*syn*–*anti* G-tetrad is not the

energetically favorable configuration of the antiparallel G-4 structure. The CD spectra of M2(5,11), M2(10,11) and M2(11,14) suggested an unstructured TBA because each one has one G-tetrad with either *syn*−*anti*−*anti*−*anti* or *anti*−*anti*−*syn*−*anti* arrangement **(Fig. 4B)**. Substitutions for dG2 and dG11 do not disturb the *syn*−*anti*−*syn*−*anti* arrangement, and M2(2,11) presents a very weak CD spectrum, suggesting a much less stable G-4 structure (**Fig. 4B**). TBA M4(2,5,11,14) and M8(1,2,5,6,10,11,14,15) present featureless CD spectra, an indication of an unstructured TBA due to the *anti*−*syn* switch (**Fig. 4C**). **Fig. 5** shows TDS data of substituted TBAs. When the antiparallel G-4 structures are conserved, the TDS results show characteristic spectral features which are consistent with the previous report [28]. These data unambiguously indicated that the selective substitutions of OMe for *syn*-dG residues disturb the *syn*−*anti*−*syn*−*anti* arrangement of the G-tetrads of the antiparallel G-4 folding topology and lead to the collapse of the TBA structure consequently.

To evaluate the folding topology and molecularity of these OMe-substituted TBAs, we also performed the electrophoresis mobility shift assay (**Fig. 6**). The native TBA migrates at the fastest rate equivalent to a 10-bp marker in K^+-gel due to its compact structure, whereas the unstructured species M8 migrates at the slowest rate similar to a 14-bp marker (**Fig. 6A**). Other substituted TBAs move differently due mainly to their structural variations. It is worth noting that all TBAs, either the native or the OMe-substituted ones, show a distinctive single band, implying that only one TBA conformer is present in each case. Tang and Shafer [45] studied the G-4 structure using 20% non-denaturing polyacrylamide gel at 4°C. Their results showed that TBA migrated at the rate equivalent to the dT13 marker; whereas ribonucleotide-substituted rTBA of parallel G-4 structure appeared a smear band between dT22 and dT27, indicating that its mobility was significantly retarded. These results indicated that the parallel G-4 structure migrates much slower than an antiparallel G-4 structure. Our gel mobility shift assay results are also in good agreement with the CD results, i.e. the native TBA, M1(2) and M(5) in K^+ solution are of an antiparallel G-4 topology, and M8 in K^+ solution is unstructured.

To further examine the structural stability of different TBA species, UV thermal melting analysis was conducted. Thermal melting and annealing curves at 295 nm of the native TBA are perfectly reversible, indicating a thermal equilibrium process. The melting temperature was determined to be 50.2°C, consistent with the data reported in a previous study [46]. M1(2) in K^+ solution also exhibits reversible melting and annealing curves, and T_m and T_a were measured at 38.7 and 38.1°C, respectively. M1(11) shows a similar thermal reversible feature with T_m and T_a of 38.8 and 38.2°C. The lack of hysteresis between denaturation and renaturation curves indicates an intramolecular formation process of G-quadruplex [47]. This conclusion is consistent with the gel analysis results. Once the *syn*-dG residues are substituted, M1(5) and M1(14) in K^+ solution show very small absorbance changes and no obvious thermal transition, indicating that they are less stable. All M2(5,11), M2(10,11) and M2(11,14), as well as M4 and M8, show flat curves without thermal transition at all. The concentration-independent behavior of melting temperatures of TBA variants in K^+ solution provides an additional proof of intramolecular G-4 structure (**Fig. 8**).

Further comparison has revealed an interesting phenomenon. When all the *syn*-dG residues were substituted by RNA, TBA was converted to a parallel G-4 structure in K^+ solution [45]. On the contrary, full substitutions of TBA with LNA in K^+ solution led to a complete destruction of the TBA structure [44]. In the present study, OMe substitutions for *syn*-dG residues also destroy the TBA structure. Thus, it strongly suggested that although RNA, LNA, and OMe share a similar *C3′-endo* sugar pucker conformation and the *anti* glycosidic angle, they do have different impacts on the TBA structure. It is probably due to the electronegativity, steric repulsion, hydrophobicity and other properties of different nucleotide derivatives. Further studies are needed.

Divalent ions Ca^{2+} and Mg^{2+} play an important role in many biological events. Ca^{2+} functions as the secondary massager to conduct intracellular signals and as a regulatory factor to control the cascade coagulation reactions as well. Mg^{2+} works as the cofactor of enzymes or as the activators to promote enzymatic activity. Literature analysis showed that almost all the experiments of TBA, including those substituted TBAs with LNA, 2′-F-ANA and UNA, have been conducted in monovalent ionic solution, but the influence of divalent ions Ca^{2+} or Mg^{2+} on the TBA G-4 structure has rarely been reported.

One previous study has explored the G-4 structure of TBA in monovalent ions (Li^+, Na^+, K^+, Rb^+, Cs^+, NH_4^+) as well as in divalent ion (Mg^{2+}, Ca^{2+}, Sr^{2+}, and Ba^{2+}) environments [48]. The native TBA in Li^+, Na^+, K^+, Cs^+, Ca^{2+}, and Mg^{2+} solutions showed similar CD spectra. The melting behavior of the TBA-ion complexes concluded that K^+, Rb^+, NH_4^+, Sr^{2+} and Ba^{2+} benefited the formation of an antiparallel G-4 structure with transition temperatures above 25°C. However, a weak complex of TBA with cations Li^+, Na^+, Cs^+, Mg^{2+}, and Ca^{2+} could only be formed at very low temperatures. Results concluded that only cations with an ionic radius of 1.3−1.5 Å could be sandwiched perfectly by two G-tetrad planes of TBA, while other cations were either too small or too large to fit in this space. This study showed that the melting temperatures of TBA in Ca^{2+} and Mg^{2+} solutions could not be determined since they did not show any thermal transitions monitored at 295 nm. The ionic radii of Na^+ and Ca^{2+} have been estimated to be ~1.0 Å, and their essential binding site for the parallel G-4

structure has been found to be the same [49]. Previous investigations have also found that Ca^{2+} could promote the intramolecular antiparallel G-4 d[$(G_4T_4)_3G_4$)] to undergo the structure transition [50,51]. Our data (**Figs. 4** and **5**) provide more experimental evidence to support this empirical rule.

In the present study, the native TBA appears to be unstructured in 50 mM Ca^{2+} solution (**Figs. 4D** and **5D**), and so are the single-OMe substituted TBAs except M1(5). Double-substituted TBAs are also unstructured (**Fig. 4E**). When the G-tetrads are substituted with OMe, their CD spectra showed a formation of a parallel G-4 structure (**Fig. 4F**). In this case, the G-tetrads are in the *anti*−*anti*−*anti*−*anti* glycosidic conformations, an energetically favored structure by parallel G-4 [52]. It is interesting to make a comparison with a previous study of the tailed TBAs, 5′-GTAGGT-TBA and 5′-TTTTTT-TBA [33]. These two TBA variants showed different CD spectra in different ion solutions. In K^+ solution, both tailed TBAs showed CD spectra similar to that of an antiparallel G-4 structure. However, in Ca^{2+} or Mg^{2+} solution, the tailed 5′-GTAGGT-TBA was of the parallel G-4 structure, whereas 5′-TTTTTT-TBA was a mixture of parallel and antiparallel structures. Unfortunately, melting temperatures of these two-tailed TBAs in the Ca^{2+} and Mg^{2+} solutions were not determined.

In Ca^{2+}-containing gel, the native TBA migrates at a much slower rate which is like the unstructured M8 in the K^+-containing gel, and M8 is significantly retarded (**Fig. 6B**). Other partially substituted TBAs migrate at the rates between the native TBA and M8. Importantly, all the native and OMe-substituted TBAs show a distinctive single band in the 20% gel, implying that only one type of G-quadruplex is formed.

We also assessed the thermal stabilities of these TBA variants in Ca^{2+} solution. The native TBA and three M1 TBAs show no thermal denaturation at all, and only M1(5) exhibits a minor thermal transition with a small hysteresis. None of the M2 TBAs show obvious thermal transition (Supplementary Fig. S2). M4, however, exhibits hysteresis property, with T_m and T_a determined to be 53.2 and 33.1°C, respectively. In general, the hysteresis of melting and annealing curves is observed under two conditions. The first situation is when the heating and cooling rates are too fast so that the transition process does not reach the thermodynamic equilibrium state, and the second situation is when the complex formation is an intermolecular process. In the present study, the hysteresis is still observable even at slower heating and cooling rates of 0.2°C/min, indicating that the M8 formation is probably an intermolecular association event in Ca^{2+} solution, since this folding process is a slower dynamic process than the unfolding one. These results also suggested that the unfolding−folding process in K^+ solution is different from that in Ca^{2+} solution.

Miyoshi *et al.* [53] have quantitatively investigated the effects of divalent cations on the antiparallel G-4 of d($G_4T_4G_4$), and showed that higher concentrations of Ca^{2+} could induce a structural transition from the antiparallel to the parallel G-4, and finally to G-wire, a highly ordered parallel G-4 structure. Other examples include a supramolecular self-assembly of d[$(TGG)_4$] induced by Mg^{2+} [54], an intermolecular G-4 of d[$(G_4T_2)_3G_4$] induced by Sr^{2+} [55], and a parallel G-4 of d($TGTG_3TGTGTGTG_3$) in the presence of Mg^{2+} and Ba^{2+} [56]. Neidle *et al.* [57] have proposed a model for higher-order telomere structure of d[$TAG_3T_2AG_3T$] and d[$AG_3(T_2AG_3)_3$]. This model reveals that the parallel strands are linked with the trinucleotide loops positioned on the outside of the G-tetrads in a propeller-like arrangement, and therefore the folded human G-4 can form a cylindrical quasi-super helix, like a G-wire, with the stacking interactions between G-tetrads [57]. Based on the kinetic and equilibrium analyses, Miyoshi *et al.* [50] concluded that at least two Ca^{2+} ions were required for the transition. The Ca^{2+} ions are located at the center of the four G-quartets or between two G-tetrads when the O6 atoms of guanine residue are accessible. The kinetic parameters also indicated that d($G_4T_4G_4$) underwent the transition through multiple steps involving the Ca^{2+} binding, isomerization, and oligomerization of d($G_4T_4G_4$). Our results showed that only TBA M8 in Ca^{2+} solution exhibits a CD spectrum of a parallel G-4 structure (**Fig. 4F**), a concentration-dependent melting temperature profile (**Fig. 8**), and a multiple-phase transition behavior (**Fig. 7**). All the results lead to the conclusion that the M8 might be present in a more stable parallel G-4 topology in Ca^{2+} solution. A recent study showed that when the TT loops were replaced by one or two guanine residues, TBA became an intermolecular parallel G-4 structure [46].

There are still debates about the contributions of enthalpy and entropy to the G-4 structure stability; however, no conclusive remarks have been derived. A previous study focusing on the molecular dynamic simulation proposed that the enthalpy favors the antiparallel G-4 structure, whereas the entropy favors the parallel form [26]. The stable G-4 structures are believed to be due to interactions within loops as well as between loops and G-quartets. This molecular dynamic simulation also predicted that entropic contributions are more significant in parallel G-4 structures where the loop flexibility is greater [26]. Bugaut and Balasubramanian [58] have observed that addition of one nucleotide led to a significant decrease in both T_m and ΔG at 37°C for the G-4 structures with a total loop length less than five nucleotides. On the other hand, any increase in loop lengths does not significantly affect the stability when the total loop length is more than five nucleotides [58]. Using G_3TTTG_3-loop-G_3TTTG_3 and G_3TTAG_3-loop-G_3TTAG_3 as model compounds (loop length = 1−12 thymine residues), a strong correlation between the total loop length and T_m was established:, i.e. the addition of one nucleotide resulted in a 2°C drop or ~0.3 kcal/mol in ΔG in K^+ solution. However, this trend was less clear in Na^+ solution [59].

Based on the melting curves, we used the non-linear least-square curve fitting method to fit the melting and annealing curves recorded at 295 nm, and calculated van't Hoff data (enthalpy and entropy) for the native TBA and OMe-substituted TBAs. As shown in **Table 2**, the OMe-substituted M1(2) and M1(11) in K^+ solution have increased the ΔH (by ~65 kJ/mol) and TΔS (by ~55 kJ/mol). However, the increased TΔS is not enough to compensate for the increased ΔH, resulting in the reduced stability (by 10 kJ/mol). In the case of M2(2,11), ΔH and TΔS were further increased by ~12.5 and ~8.0 kJ/mol, respectively, leading to a much less stable structure. These results concluded that thermal stability of the OMe-substituted TBAs is an enthalpy-driven event. In Ca^{2+} solution, M4 showed the two-phase transition, and the calculated values of ΔH and TΔS were close to that of the native TBA. In the case of M8, a higher melting temperature might indicate the formation of parallel G-4 structure.

Cancer has become the first threat to human health worldwide. Although chemotherapy and radiotherapy can deliver promising treatment results, their toxicity and drug resistance have become two major obstacles to achieve the desired success. Using oligonucleotides with particular G-quadruplex structures as therapeutic agents have been proposed as new types of treatment strategy. Two strategies have been proposed. One is to prepare oligonucleotides the sequences of which are the same as that of the targeted promoters and to terminate the transcription once bound to the promoter of the targeted genes [60]. Another one is to design novel G-4 structures which possess high binding affinities with regulatory proteins and to interfere with the signal transduction pathways [61,62]. To guarantee the effectiveness of these approaches, several technical problems have to be solved:, i.e. how to ensure the correct folding topology of these G-4 forming sequences, how to reduce the off-targeting efficiency, and how to enhance their structural stability to resist enzymatic digestion in blood circulation system. Nucleotide derivatives could provide promising solution in this regard, since they demonstrate a great diversity of structures and physicochemical properties. As revealed in this study and other investigations, different nucleotide derivatives can modulate the G-4 topologies, structural stabilities and binding affinities of TBA. Further evidence has also shown a correlation between the biological activity and the selected substitutions. All these results pinpoint the potential applications of the nucleotide derivatives substituted G-quadruplexes in biological and medical research.

To understand the effect of the sugar pucker conformation and the cations on the TBA G-4 folding topology and structural stability, we prepared a group of TBA variants which possess OMe substitutions at the selected positions, and used CD, TDS, UV stability analysis, electrophoresis mobility shift assay and thermodynamic analysis to examine these TBAs in K^+ or Ca^{2+} environment. In K^+ solution, OMe substitutions for *syn*-dG residues destabilized the G-quadruplex structure, while substitutions for *anti*-dG residues preserved possibly the G-quadruplex. Substitutions for more residues exhibited a negative impact on the TBAs' stability. In contrast, in Ca^{2+} solution, the native TBA was unstructured due probably to the smaller radium of Ca^{2+}, while other single-substituted and double-substituted TBAs showed no structure at all. A G-tetrad substitution induces a parallel G-4 formation and two G-tetrad substitutions were speculated to form a more stable parallel G-4 structure. Thermodynamic analyses showed that the G-4 structures of different substituted TBAs in K^+ and Ca^{2+} environments were enthalpically favored. The structural variation of TBAs in different ionic environments enriches our understanding about the TBA and other G-quadruplex formation, and these results and conclusions could benefit the design of novel G-quadruplexes for biomedical applications.

Supplementary Data

Supplementary Data is available at *ABBS* online.

Funding

This work was supported by a grant from the National Natural Science Foundation of China (81371896).

References

1. Blackburn EH. Structure and function of telomeres. Nature 1991, 350: 569–573.
2. Lee JY, Okumus B, Kim DS and Ha T. Extreme conformational diversity in human telomeric DNA. Proc Natl Acad Sci USA 2005, 102: 18938–18943.
3. Xu Y, Sato H, Sannohe Y, Shinohara K and Sugiyama H. Stable lariat formation based on a G-quadruplex scaffold. J Am Chem Soc 2008, 130: 16470–16471.
4. Brooks TA, Kendrick S and Hurley L. Making sense of G-quadruplex and i-motif functions in oncogene promoters. FEBS J 2010, 277: 3459–3469.
5. Fernando H, Reszka AP, Huppert J, Ladame S, Rankin S and Venkitaraman AR. A conserved quadruplex motif located in a transcription activation site of the human c-kit oncogene. Biochemistry 2006, 45: 7854–7860.
6. Kumari S, Bugaut A and Balasubramanian S. Position and stability are determining factors for translation repression by an RNA G-quadruplex-forming sequence within the 5′ UTR of the NRAS proto-oncogene. Biochemistry 2008, 47: 12664–12669.
7. Morris MJ and Basu S. An unusually stable G-quadruplex within the 5′-UTR of the MT3 matrix metalloproteinase mRNA represses translation in eukaryotic cells. Biochemistry 2009, 48: 5313–5319.
8. Rangan A, Fedoroff OY and Hurley LH. Induction of duplex to G-quadruplex transition in the c-myc promoter region by a small molecule. J Biol Chem 2001, 276: 4640–4646.
9. Tornaletti S. Transcriptional processing of G4 DNA. Mol Carcinog 2009, 48: 326–335.
10. Macaya RF, Schultze P, Smith FW, Roe JA and Feigon J. Thrombin-binding DNA aptamer forms a unimolecular quadruplex structure in solution. Proc Natl Acad Sci USA 1993, 90: 3745–3749.

11. Kelly JA, Feigon J and Yeates TO. Reconciliation of the X-ray and NMR structures of the thrombin-binding aptamer d(GGTTGGTGTGGTTGG). J Mol Biol 1996, 256: 417–422.
12. Griffin LC, Tidmarsh GF, Bock LC, Toole JJ and Leung LL. *In vivo* anticoagulant properties of a novel nucleotide-based thrombin inhibitor and demonstration of regional anticoagulation in extracorporeal circuits. Blood 1993, 81: 3271–3276.
13. Padmanabhan K, Padmanabhan KP, Ferrara JD, Sadler JE and Tulinsky A. The structure of alpha-thrombin inhibited by a 15-mer single-stranded DNA aptamer. J Biol Chem 1993, 268: 17651–17654.
14. Bonifacio L, Church FC and Jarstfer MB. Effect of locked-nucleic acid on a biologically active g-quadruplex. A structure–activity relationship of the thrombin aptamer. Int J Mol Sci 2008, 9: 422–433.
15. Agarwal T, Kumar S and Maiti S. Unlocking G-quadruplex: effect of unlocked nucleic acid on G-quadruplex stability. Biochimie 2011, 93: 1694–1700.
16. Jensen TB, Henriksen JR, Rasmussen BE, Rasmussen LM, Andresen TL and Wengel J . Thermodynamic and biological evaluation of a thrombin binding aptamer modified with several unlocked nucleic acid (UNA) monomers and a 2′-C-piperazino-UNA monomer. Bioorg Med Chem 2011, 19: 4739–4745.
17. Kalota A, Karabon L, Swider CR, Viazovkina E, Elzagheid M and Damha MJ. 2′-Deoxy-2′-fluoro-beta-D-arabinonucleic acid (2′F-ANA) modified oligonucleotides (ON) effect highly efficient, and persistent, gene silencing. Nucleic Acids Res 2006, 34: 451–461.
18. Matsugami A, Xu Y, Noguchi Y, Sugiyama H and Katahira M. Structure of a human telomeric DNA sequence stabilized by 8-bromoguanosine substitutions, as determined by NMR in a K^+ solution. FEBS J 2007, 274: 3545–3556.
19. Goji S and Matsui J. Direct detection of thrombin binding to 8-bromodeoxyguanosine-modified aptamer: effects of modification on affinity and kinetics. J Nucleic Acids 2011, 2011:316079.
20. Prakash TP and Bhat B. 2′-Modified oligonucleotides for antisense therapeutics. Curr Top Med Chem 2007, 7: 641–649.
21. Majlessi M, Nelson NC and Becker MM. Advantages of 2′-*O*-methyl oligoribonucleotide probes for detecting RNA targets. Nucleic Acids Res 1998, 26: 2224–2229.
22. Kierzek E, Ciesielska A, Pasternak K, Mathews DH, Turner DH and Kierzek R. The influence of locked nucleic acid residues on the thermodynamic properties of 2′-*O*-methyl RNA/RNA heteroduplexes. Nucleic Acids Res 2005, 33: 5082–5093.
23. Burmeister PE, Lewis SD, Silva RF, Preiss JR, Horwitz LR and Pendergrast PS. Direct *in vitro* selection of a 2′-*O*-methyl aptamer to VEGF. Chem Biol 2005, 12: 25–33.
24. Chen AK, Behlke MA and Tsourkas A. Sub-cellular trafficking and functionality of 2′-*O*-methyl and 2′-*O*-methyl-phosphorothioate molecular beacons. Nucleic Acids Res 2009, 37: e149.
25. Laursen MB, Pakula MM, Gao S, Fluiter K, Mook OR and Baas F. Utilization of unlocked nucleic acid (UNA) to enhance siRNA performance *in vitro* and *in vivo*. Mol Biosyst 2010, 6: 862–870.
26. Hazel P, Huppert J, Balasubramanian S and Neidle S. Loop-length-dependent folding of G-quadruplexes. J Am Chem Soc 2004, 126: 16405–16415.
27. Davis JT. G-quartets 40 years later: from 5′-GMP to molecular biology and supramolecular chemistry. Angew Chem Int Ed Engl 2004, 43: 668–698.
28. Mergny JL, Li J, Lacroix L, Amrane S and Chaires JB. Thermal difference spectra: a specific signature for nucleic acid structures. Nucleic Acids Res 2005, 33: e138.
29. Zheng YT, Zhu JH, Ma G, Zhu Q, Yang P and Tan B. Preclinical assessment of the distribution, metabolism, and excretion of *S*-propargyl-cysteine, a novel H2S donor, in Sprague-Dawley rats. Acta Pharmacol Sin 2012, 33: 839–844.
30. Cantor CR. Photo-cross-linking studies of nucleic acid structure. Ann N Y Acad Sci [Research Support, US Gov't, Non-P.H.S. Research Support, U.S. Gov't, P.H.S.] 1980, 346: 379–385.
31. Nagatoishi S, Tanaka Y and Tsumoto K. Circular dichroism spectra demonstrate formation of the thrombin-binding DNA aptamer G-quadruplex under stabilizing-cation-deficient conditions. Biochem Biophys Res Commun 2007, 352: 812–817.
32. Dapic V, Abdomerovic V, Marrington R, Peberdy J, Rodger A and Trent JO. Biophysical and biological properties of quadruplex oligodeoxyribonucleotides. Nucleic Acids Res 2003, 31: 2097–2107.
33. De Rache A, Kejnovska I, Vorlickova M and Buess-Herman C. Elongated thrombin binding aptamer: a G-quadruplex cation-sensitive conformational switch. Chemistry 2012, 18: 4392–4400.
34. Marky LA and Breslauer KJ. Calculating thermodynamic data for transitions of any molecularity from equilibrium melting curves. Biopolymers 1987, 26: 1601–1620.
35. Wang KY, McCurdy S, Shea RG, Swaminathan S and Bolton PH. A DNA aptamer which binds to and inhibits thrombin exhibits a new structural motif for DNA. Biochemistry 1993, 32: 1899–1904.
36. Virno A, Randazzo A, Giancola C, Bucci M, Cirino G and Mayol L. A novel thrombin binding aptamer containing a G-LNA residue. Bioorg Med Chem 2007, 15: 5710–5718.
37. Saneyoshi H, Mazzini S, Avino A, Portella G, Gonzalez C and Orozco M. Conformationally rigid nucleoside probes help understand the role of sugar pucker and nucleobase orientation in the thrombin-binding aptamer. Nucleic Acids Res 2009, 37: 5589–5601.
38. Rujan IN, Meleney JC and Bolton PH. Vertebrate telomere repeat DNAs favor external loop propeller quadruplex structures in the presence of high concentrations of potassium. Nucleic Acids Res [Research Support, U.S. Gov't, P.H.S.] 2005, 33: 2022–2031.
39. Olsen CM and Marky LA. Monitoring the temperature unfolding of G-quadruplexes by UV and circular dichroism spectroscopies and calorimetry techniques. Methods Mol Biol [Research Support, Non-U.S. Gov't Research Support, U.S. Gov't, Non-P.H.S.] 2010, 608: 147–158.
40. Ambrus A, Chen D, Dai J, Bialis T, Jones RA and Yang D. Human telomeric sequence forms a hybrid-type intramolecular G-quadruplex structure with mixed parallel/antiparallel strands in potassium solution. Nucleic Acids Res 2006, 34: 2723–2735.
41. Pasternak A, Hernandez FJ, Rasmussen LM, Vester B and Wengel J. Improved thrombin binding aptamer by incorporation of a single unlocked nucleic acid monomer. Nucleic Acids Res 2011, 39: 1155–1164.
42. Peng CG and Damha MJ. G-quadruplex induced stabilization by 2′-deoxy-2′-fluoro-D-arabinonucleic acids (2′F-ANA). Nucleic Acids Res 2007, 35: 4977–4988.
43. Wilson C and Keefe AD. Building oligonucleotide therapeutics using non-natural chemistries. Curr Opin Chem Biol 2006, 10: 607–614.
44. Randazzo A, Esposito V, Ohlenschlager O, Ramachandran R, Virgilio A and Mayol L. Structural studies on LNA quadruplexes. Nucleosides Nucleotides Nucleic Acids 2005, 24: 795–800.
45. Tang CF and Shafer RH. Engineering the quadruplex fold: nucleoside conformation determines both folding topology and molecularity in guanine quadruplexes. J Am Chem Soc 2006, 128: 5966–5973.
46. Avino A, Portella G, Ferreira R, Gargallo R, Mazzini S and Gabelica V. Specific loop modifications of the thrombin-binding aptamer trigger the formation of parallel structures. FEBS J 2013, 281: 1085–1099.
47. Mergny JL, Phan AT and Lacroix L. Following G-quartet formation by UV-spectroscopy. FEBS Lett 1998, 435: 74–78.
48. Kankia BI and Marky LA. Folding of the thrombin aptamer into a G-quadruplex with Sr(2+): stability, heat, and hydration. J Am Chem Soc 2001, 123: 10799–10804.

49. Hardin CC, Watson T, Corregan M and Bailey C. Cation-dependent transition between the quadruplex and Watson–Crick hairpin forms of d(CGCG3GCG). Biochemistry 1992, 31: 833–841.
50. Miyoshi D, Nakao A and Sugimoto N. Structural transition from antiparallel to parallel G-quadruplex of d(G4T4G4) induced by Ca^{2+}. Nucleic Acids Res 2003, 31: 1156–1163.
51. Dominick PK and Jarstfer MB. A conformationally constrained nucleotide analogue controls the folding topology of a DNA g-quadruplex. J Am Chem Soc 2004, 126: 5050–5051.
52. Tsourkas A, Behlke MA and Bao G. Hybridization of 2′-*O*-methyl and 2′-deoxy molecular beacons to RNA and DNA targets. Nucleic Acids Res 2003, 31: 5168–5174.
53. Miyoshi D, Nakao A, Toda T and Sugimoto N. Effect of divalent cations on antiparallel G-quartet structure of d(G4T4G4). FEBS Lett 2001, 496: 128–133.
54. Chen FM. Supramolecular self-assembly of d(TGG)4, synergistic effects of K^+ and Mg^{2+}. Biophys J 1997, 73: 348–356.
55. Chen FM. Sr^{2+} facilitates intermolecular G-quadruplex formation of telomeric sequences. Biochemistry 1992, 31: 3769–3776.
56. Venczel EA and Sen D. Parallel and antiparallel G-DNA structures from a complex telomeric sequence. Biochemistry 1993, 32: 6220–6228.
57. Parkinson GN, Lee MP and Neidle S. Crystal structure of parallel quadruplexes from human telomeric DNA. Nature 2002, 417: 876–880.
58. Bugaut A and Balasubramanian S. A sequence-independent study of the influence of short loop lengths on the stability and topology of intramolecular DNA G-quadruplexes. Biochemistry 2008, 47: 689–697.
59. Guedin A, Gros J, Alberti P and Mergny JL. How long is too long? Effects of loop size on G-quadruplex stability. Nucleic Acids Res 2010, 38: 7858–7868.
60. Balasubramanian S, Hurley LH and Neidle S. Targeting G-quadruplexes in gene promoters: a novel anticancer strategy? Nat Rev Drug Discov 2011, 10: 261–275.
61. Gatto B, Palumbo M and Sissi C. Nucleic acid aptamers based on the G-quadruplex structure: therapeutic and diagnostic potential. Curr Med Chem 2009, 16: 1248–1265.
62. Teng Y, Girvan AC, Casson LK, Pierce WM, Jr., Qian M and Thomas SD. AS1411 alters the localization of a complex containing protein arginine methyltransferase 5 and nucleolin. Cancer Res 2007, 67: 10491–10500.